NANO LETTERS

Letter

pubs.acs.org/NanoLett

Extreme Light Absorption in Thin Semiconductor Films Wrapped around Metal Nanowires

Sander A. Mann and Erik C. Garnett*

Center for Nanophotonics, FOM Institute AMOLF, Science Park Amsterdam 104, 1098 XG Amsterdam, The Netherlands

Supporting Information

ABSTRACT: Metallic and dielectric nanostructures have highly tunable resonances that have been used to increase light absorption in a variety of photovoltaic materials and device structures. Metal nanowires have also emerged as a promising candidate for high-performance transparent electrodes for local contacts. In this Letter we propose combining these electrical and optical functions. As a first step, we use rigorous solutions to Maxwell's equations to demonstrate theoretically extreme absorption in semiconductor thin films wrapped around metal nanowires. We show that there are two key principles underlying this extraordinary light trapping effect: (1) maximizing the absorption of each individual resonance by ensuring it is critically coupled and (2) increasing the total number of degenerate resonances. Inserting a metal core into a semiconductor nanowire creates such a degeneracy: polarization-dependent Mie resonances are transformed into polarization-independent Fabry-Pérot-like resonances. We demonstrate that, by reducing the polarization sensitivity and increasing the number of critically coupled modes, this hybrid coaxial nanowire geometry substantially outperforms solid semiconducting nanowires, even though the semiconductor volume is significantly reduced. These results suggest that metal nanowires with semiconductor shells might be ideal building blocks for photovoltaic and solar fuel applications.

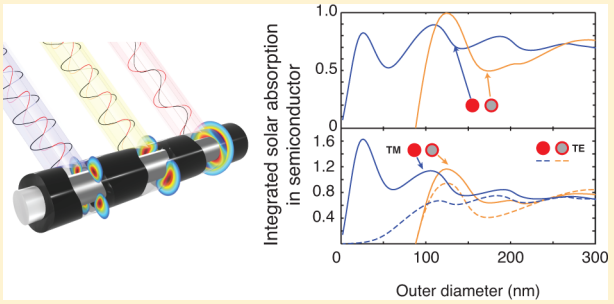

KEYWORDS: *Nanowires, solar cells, light trapping, critical coupling, nanophotonics, transparent electrodes, solar fuels, water-splitting*

Photovoltaics provide a clean and abundant source of energy but are currently too expensive to compete with grid electricity prices.[1−3] Wafer-based silicon solar cells can have very high conversion efficiencies but also require extensive material purification and batch processing which lead to high manufacturing costs and low throughputs.[4] Thin-film cadmium telluride solar cells have extremely low manufacturing costs and high throughputs, but due to their somewhat lower efficiencies, the installed cost is similar to that of crystalline silicon. This trade-off exists for many solar technologies: thick semiconductor layers are needed to absorb all of the above band gap photons, while thin layers are needed to efficiently extract carriers.[4] However, an ideal solar cell would achieve both: near unity absorption in thin layers. Combined with the reduction of material and fabrication costs, this indicates that efficient light trapping is essential for cheap photovoltaics.

Over the past decade, light trapping research has shifted focus from large-scale texturing intended to increase scattering within the ray-optics limit to nanoscale patterning designed to confine photons in the active layer via optical resonances and waveguide modes.[5−9] This shift has been enabled by the flourishing field of nanophotonics, which has demonstrated impressive control over photon confinement using both metallic[10,11] and dielectric resonators.[12] By making the resonator from an absorbing material, the high field intensities inside the structure can directly contribute to improved absorption[9,13] and even photocurrent.[14] The nanowire geometry is particularly interesting as it allows for excellent charge extraction[15−17] and a large optical cross section.[18,19] Although single crystalline semiconducting nanowires have already shown excellent charge extraction properties, metal nanowires have higher conductivity and should therefore provide a more effective local contact. In fact, metal nanowire networks have already been demonstrated as high-performance transparent electrodes in touch-screen, display, and photovoltaic applications.[20] One of the limiting factors for such next generation electrodes is the parasitic optical absorption loss caused by reflected and scattered light.[18,21,22] Here we propose eliminating these so-called shadowing losses by embedding metal nanowires in an ultrathin semiconducting shell. Although this geometry has been studied before for photovoltaics[23] and metamaterials,[24] the parameter space showing optimal absorption (ultrathin shells) was not explored. We show that this core−shell geometry efficiently couples light normally reflected and scattered by the metal core into photonic resonances in the shell. This hybrid core−shell geometry leads to an absorption efficiency ($\langle\eta_{abs}\rangle_{AM1.5}$) equivalent to nearly 100% (normalized to the nanowire's projected diameter) of

Received: April 2, 2013
Revised: June 6, 2013

   dx.doi.org/10.1021/nl401179h | *Nano Lett.* XXXX, XXX, XXX−XXX

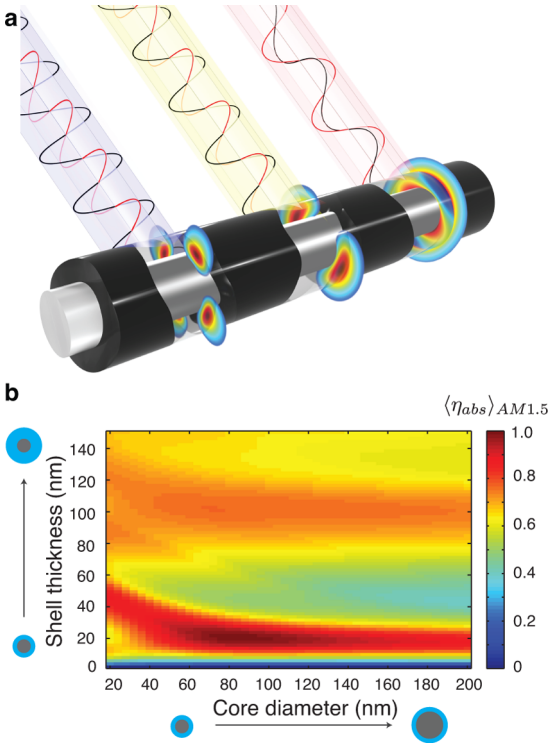

Figure 1. (a) Schematic view of a metal-semiconductor core−shell nanowire, with from left to right the TM_{21}, TM_{11}, and TE_{11} resonances, excited at different wavelengths. (b) The fraction of absorbed above-band gap photons in the amorphous silicon shell for a wide variety of configurations.

photons with an energy above that of the band gap (averaged over the AM1.5 spectrum, Figure 1). As with previous studies of nanowire optical antennas (both theoretical and experimental), these results cannot be simply translated to large area devices due to the well-known antenna effect and coupling between adjacent nanoscale resonators.[14,18,19,25,26] However, we can directly compare our absorption results with those of other isolated nanowire resonators. Here we demonstrate that horizontal metal nanowires with ultrathin shells show higher semiconductor absorption than solid nanowires. This exceptional performance arises because our proposed structures provide the ability to critically couple multiple resonances in both polarizations just above the band gap energy. Therefore we show that this geometry combines the absorption benefits of ultrathin semiconductor layers recently observed in planar structures[27,28] with the high optical cross sections caused by the antenna effect in nanowires to provide outstanding absorption with less material, while integrating a transparent electrode contact.

We begin our discussion by using a solid semiconductor nanowire as a simple model system to illustrate the importance of critically coupled resonances and polarization degeneracy. Next we show how inserting a metal core into a semiconducting nanowire transforms polarization-dependent Mie resonances into nearly polarization-independent Fabry-Pérot-like resonances. Finally, we compare the core−shell nanowire to a solid semiconductor nanowire to elucidate how an additional critically coupled resonance in the TE polarization leads to enhanced absorption.

Our absorption calculations use Mie theory, a powerful and well-known tool to analyze the optical properties of (infinitely long) nanowires.[29] In Mie theory, the total scattering and absorption cross sections in each polarization are expressed as a summation:

$$C_{\mathrm{abs}}^{\mathrm{TE}} = C_{\mathrm{abs},0}^{\mathrm{TE}} + 2\sum_{m=1}^{\infty} C_{\mathrm{abs},m}^{\mathrm{TE}} \quad (1)$$

where $C_{\mathrm{abs},m}^{\mathrm{TE}}$ is the absorption cross section for TE polarized light in the mth angular momentum channel. In other words, m describes the number of angular nodes in the field distributions. Note that channels with $m \geq 1$ contribute twice as much to the total cross section as the lowest order, $m = 0$ channel, due to degeneracy in the azimuthal phase (clockwise and counterclockwise propagation). Hereafter we will refer to the individual channels as TE_m and TM_m. Within each channel there are "leaky mode resonances", TE_{ml} and TM_{ml}, which have previously been shown to correspond to peaks in the scattering and absorption spectra of nanowires.[5,30] The additional index (subscript l) that defines each of these resonances describes the

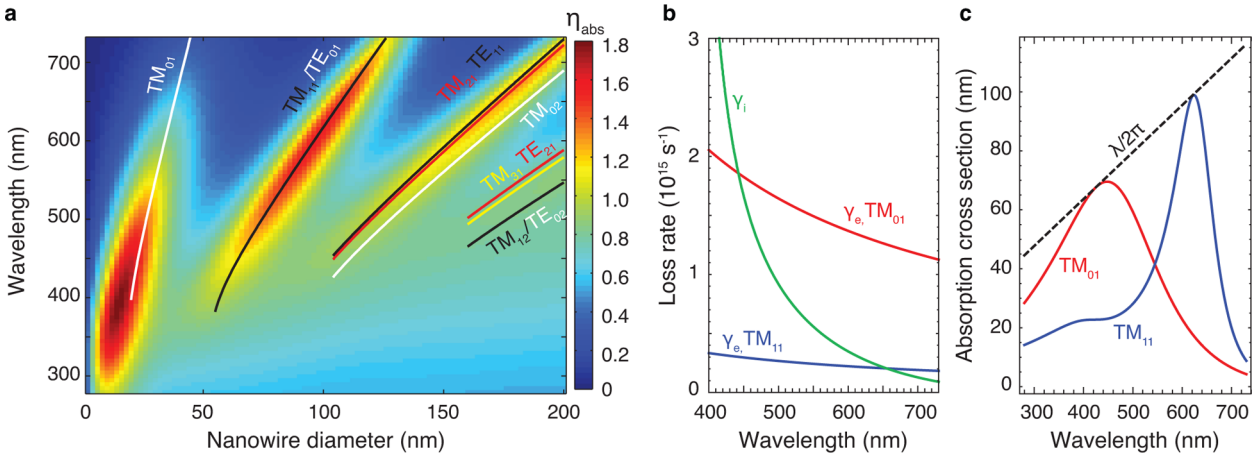

Figure 2. (a) 2D color plot of the absorption efficiency for a range of wavelengths and a-Si nanowire diameters. The white, black, red, and yellow lines correspond to resonances (see SI for details). (b) The absorption loss rate γ_i (green) and radiative loss rates γ_e for the TM_{01} (red) and TM_{11} (blue) resonances. The intersection points indicate where the resonances are critically coupled. (c) Absorption cross sections for the TM_{01} (red) and TM_{11} (blue) resonances in 22 and 102 nm diameter a-Si nanowires, respectively. The dashed line is the fundamental absorption limit for a single channel, $\lambda/2\pi$.

dx.doi.org/10.1021/nl401179h | *Nano Lett.* XXXX, XXX, XXX−XXX

number of radial field maxima within the nanowire. This notation is similar to the one used for atomic orbitals to designate principle and angular quantum numbers, which also are related to the number of radial and angular nodes, respectively. These geometrical resonances occur for fixed values of nk_0r, where n is the refractive index of the nanowire material, k_0 is the free space wavevector, and r is the radius of the cylinder.[31] Thus, one can tune the resonant wavelength by changing the diameter of the nanowire. This is clearly visible in Figure 2a, where the unpolarized absorption efficiency spectrum of an amorphous silicon nanowire under normal incidence is shown as a function of the nanowire diameter.

The absorption efficiency is defined as (see Supporting Information for details):

$$\eta_{abs} = \frac{C_{abs}}{C_{geo}} = \frac{k_0}{2r_0E_0^2}\int_0^{2\pi}\int_0^{r_0}\varepsilon''(r)|\mathbf{E}(r,\varphi)|^2 r\ \mathrm{d}r\ \mathrm{d}\varphi \tag{2}$$

where C_{abs} and C_{geo} are the absorption and geometric cross sections, respectively, r_0 is the radius of the nanowire, $\varepsilon''(r)$ is the imaginary part of the relative permittivity, E_0 is the incident electric field amplitude, and $\mathbf{E}$ is the electric field. All dielectric functions used in this work come from Palik.[32] The white, black, red, and yellow lines in Figure 2a come from mode-solver calculations for the zeroth, first, second, and third order resonances, respectively (see Supporting Information). Note that in cylindrical coordinates the TM_1 and TE_0 channels are degenerate.

The absorption efficiency of a specific resonance is not constant for a given nk_0r value, but always has a maximum at a particular diameter/wavelength combination (Figure 2a, 16/400 nm for TM_{01}, 110/600 nm for TM_{11}/TE_{01}). To understand this behavior, we turn to temporal coupled mode theory,[33,34] which shows us that the absorption cross section for any single resonance in cylindrical coordinates is:[35]

$$C_{abs,m,l} = \frac{2\lambda}{\pi}\frac{\gamma_e\gamma_i}{(\omega-\omega_0)^2+(\gamma_e+\gamma_i)^2} \tag{3}$$

Here λ is the wavelength, ω is the frequency, ω_0 is the resonant frequency, and γ_e and γ_i are the radiative and absorption loss rates of the resonator. The absorption cross section thus reaches a maximum on resonance ($\omega = \omega_0$), when $\gamma_e = \gamma_i$:

$$C_{abs,max}^{TE} = \frac{\lambda}{2\pi} \tag{4}$$

This condition is called critical coupling: the phase and amplitude of the incident and scattered waves are matched to yield complete destructive interference. This leads to the highest energy inside the cavity and hence to the maximum absorption cross section. The fundamental limit to absorption in a single channel can also be derived starting from Mie theory.[36]

To illustrate that the absorption efficiency peaks correspond to critical coupling, we show the radiative loss rates for the TM_{01} and TM_{11} resonances and the absorption loss rate for a-Si in Figure 2b (see Supporting Information for calculation details). The resonances are critically coupled where the loss rates are equal. For further illustration, Figure 2c shows the absorption spectrum of the critically coupled TM_{01} and TM_{11} resonances plotted together with the fundamental limit to absorption in a single channel ($\lambda/2\pi$, dashed line). Although previously it has been shown that a single resonance contributes most to broadband absorption in the extreme overcoupling limit ($\gamma_e \gg \gamma_i$),[37] this is not necessarily the case for nanowires because the loss rates are connected: overcoupling can only be achieved by simultaneously significantly decreasing the absorption loss rate (see Figure 2b).

Note that the higher radiative loss rate for the TM_{01} resonance is directly related to the broader bandwidth in Figure 2c. All higher order resonances have radiative loss rates much lower than that of the TM_{01} mode. Paradoxically, this means that for these higher order modes, *absorption in the semiconductor increases when the absorption coefficient decreases*. This highly counterintuitive result means that these optical resonances are especially effective at improving absorption in exactly the spectral regions that can benefit the most from light trapping (for example near the band edge).

So far we have discussed single resonances that contribute to a finite absorption band in only one polarization, but in photovoltaic and solar fuel applications we want to achieve broadband absorption in both polarizations. For a given geometry we therefore calculate the integrated weighted absorption efficiency over the solar spectrum:

$$\langle\eta_{abs}\rangle_{AM1.5} = \frac{\int F_s(\lambda)\eta_{abs}(\lambda)\ \mathrm{d}\lambda}{\int F_s(\lambda)\ \mathrm{d}\lambda} \tag{5}$$

Here η_{abs} is given by eq 2, and $F_s(\lambda)$ is the photon flux density in the AM1.5 solar spectrum.[38] The weighted absorption efficiency reflects the total number of photons absorbed in a single nanowire compared to the total above band gap photon flux through the geometrical cross section. As noted earlier, the absorption cross section in a single nanowire can exceed the geometrical cross section, due to the well-known antenna effect in subwavelength structures.[39] This benefit becomes more complex in large-scale nanowire array devices where coupling must also be considered.

Figure 3a shows the weighted absorption efficiency for a solid a-Si nanowire as a function of the nanowire diameter (in red). We integrated over the solar spectrum from 280 to 730 nm (1.7 to 4.4 eV), which are the shortest wavelengths in the AM1.5 solar spectrum and the band gap of a-Si, respectively. The peaks that appear at approximately 25, 110, and 180 nm diameters roughly correspond to subsequent resonances reaching critical coupling: first the TM_{01}, then the degenerate TM_{11}/TE_{01}, and so forth. A maximum weighted absorption of 0.9 is achieved when the TM_{11}/TE_{01} resonance is critically coupled (110 nm diameter). While the TM_{01} resonance absorbs extremely efficiently at small diameters, in that size range there is no absorption in the TE polarization (solid and dashed blue curves in Figure 3a respectively). This emphasizes the importance of good response in both polarizations. Furthermore, below 200 nm a solid nanowire is more strongly absorbing in the TM polarization because the TE_0 channel only contributes once to the absorption cross section (singly degenerate, eq 1), while the TM_1 contributes twice (doubly degenerate, eq 1).

A key strategy to enhance the absorption efficiency of a nanostructure is to increase the number of supported resonances while maintaining the same particle size.[30] This strategy is most effective when one maximizes the number of resonances that are critically coupled. Here, we will show that the enhanced absorption in a core−shell nanowire is caused by exactly this effect. To calculate the optical properties we extended Mie theory for cylinders to core−shell nanowires (see Supporting Information). Note that we want to maximize

dx.doi.org/10.1021/nl401179h | Nano Lett. XXXX, XXX, XXX−XXX

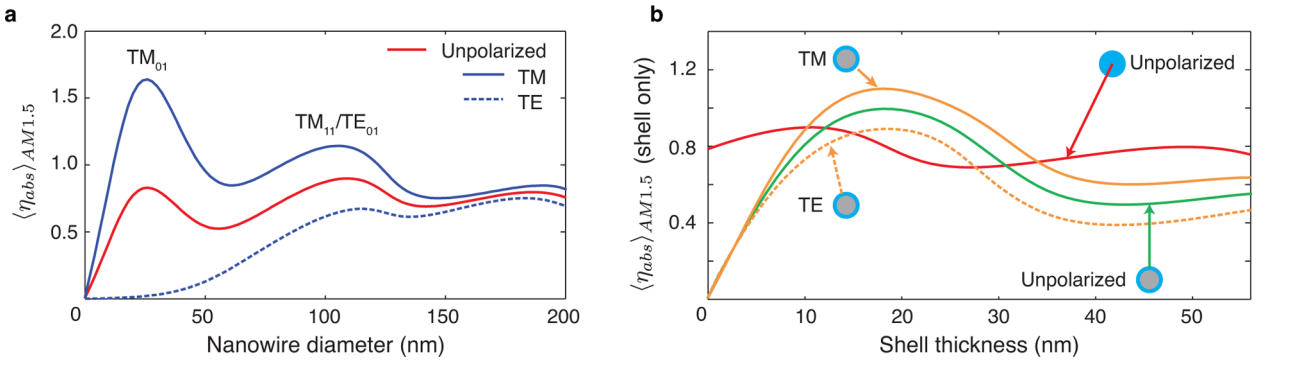

Figure 3. (a) Weighted absorption efficiency of a solid a-Si nanowire for unpolarized light (red), in TM (blue, solid) and TE (blue, dashed), as a function of diameter. The peaks correspond to critically coupled resonances. (b) The weighted absorption efficiency in an a-Si shell wrapped around an 88 nm diameter Ag nanowire as a function of shell thickness for unpolarized light (green), in TM (orange, solid) and in TE (orange, dashed). The red curve is the unpolarized weighted absorption efficiency in a solid a-Si nanowire with the same outer diameter (i.e., from 88 to 200 nm).

absorption in the shell because absorption in the metal core does not contribute to photocurrent generation. By changing the integration limits in eq 2, we can separate the desired shell absorption (plotted in Figure 3b) from the parasitic core absorption (in all cases normalizing to the outer diameter of the core–shell to keep a constant input photon flux). An unpolarized weighted absorption efficiency of 1 is observed at a shell thickness of only 18 nm, coated on an 88 nm diameter silver core (Figure 3b, green). This extraordinary absorption is higher than what can be attained in solid semiconducting nanowires (red, Figure 3a and b). By comparing the dashed curves from Figures 3a and b, it becomes clear that the absorption efficiency boost stems primarily from enhanced absorption in the TE polarization.

To understand why absorption increases in the core–shell structure despite the significant decrease in semiconductor volume, it is instructive to examine the optical properties of core–shell nanowires. Ignoring the plasmon resonance for now (assuming TM polarization), the core–shell structure supports Mie resonances when the metal core radius a is smaller than b/n, where b is the outer radius and n the real refractive index of the shell.[40] Essentially this means that, below this threshold, introducing a metal core does not perturb the normal optical resonances that exist in a solid semiconducting nanowire. However, when the inner diameter a is larger than this threshold, the standard Mie modes are strongly perturbed and begin to have Fabry-Pérot-like characteristics.[40] In a geometrical optics picture, the difference between the two regimes is that in the latter light reflects off of the metal core, while in the former it reflects only off of the semiconductor–air interface. Interestingly, such a cylindrical Fabry-Pérot cavity is very closely related to the planar structure, a phenomenon observed and explained before for coaxial nanowires.[41]

Under normal incidence a planar Fabry-Pérot cavity has no polarization sensitivity: each leaky mode resonance is polarization-degenerate. Surprisingly, even though in the cylindrical configuration a localized plasmon is supported in TE, this polarization degeneracy can still hold (Figure 4). In this example the metal core diameter is made large (180 nm) both to place the structure in the Fabry-Pérot regime and to minimize ohmic losses in the metal core (see Supporting Information). Simply put, in both polarizations the metal nanowire acts as a reflector for the Fabry-Pérot cavity even though in TE it supports a plasmon resonance. For large core diameters, the plasmon is primarily damped via scattering,

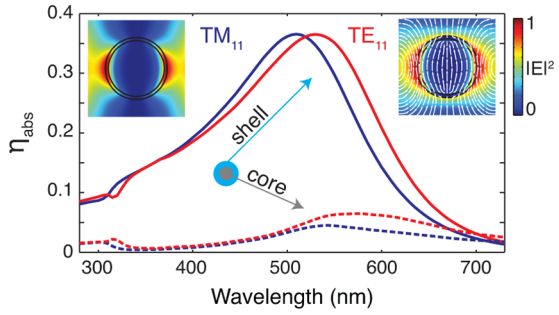

Figure 4. Absorption efficiency in TM$_{11}$ (blue) and TE$_{11}$ (red) for a 180 nm silver core with a 10 nm a-Si shell. The near-degeneracy indicates the Fabry-Pérot-like behavior. The solid lines indicate absorption in the shell, the dashed lines absorption in the core. The insets show the electric field intensities (with the stream plot indicating the direction of the field) for the TM$_{11}$ (left) and TE$_{11}$ (right) resonances.

which feeds light back into the cavity. However, even in the best case the plasmon does lead to some parasitic absorption, which slightly redshifts the TE$_{11}$ compared to the TM$_{11}$ resonance, breaking the degeneracy.

In cylindrical coordinates the TM$_1$ and TE$_0$ channels are degenerate. Therefore, the Fabry-Pérot-like behavior in core–shell nanowires described above leads to overlapping TE$_{01}$ and TE$_{11}$ resonances. This behavior is distinctly different from planar and solid nanowire systems where TE$_{01}$ and TE$_{11}$ resonances (TE$_0$ and TE$_1$ in the planar case) are always spectrally separated. Figure 5a shows the absorption efficiency spectra in the TE polarization for the most efficiently absorbing solid (110 nm diameter, left) and core–shell (88 nm diameter core, 18 nm thick shell, right) nanowires, respectively. In the solid nanowire, absorption stems primarily from the critically coupled TE$_{01}$ resonance (blue). It therefore cannot exceed the single channel absorption limit (dashed line). In the core–shell nanowire, the TE$_{01}$ and TE$_{11}$ modes overlap, causing the absorption peak to be significantly higher than the single channel limit. It is important to note that in this optimal configuration there is still a small amount of light lost to absorption in the metal (Figure 5b). In the TM polarization, absorption in the solid and core–shell nanowires is almost the same: in both cases the TM$_{11}$ resonance dominates (see Supporting Information). These results are not limited to a-Si; silver nanowires with a CdTe shell show very similar behavior, although the optimal shell thickness is 46 nm due to a lower

dx.doi.org/10.1021/nl401179h | Nano Lett. XXXX, XXX, XXX–XXX

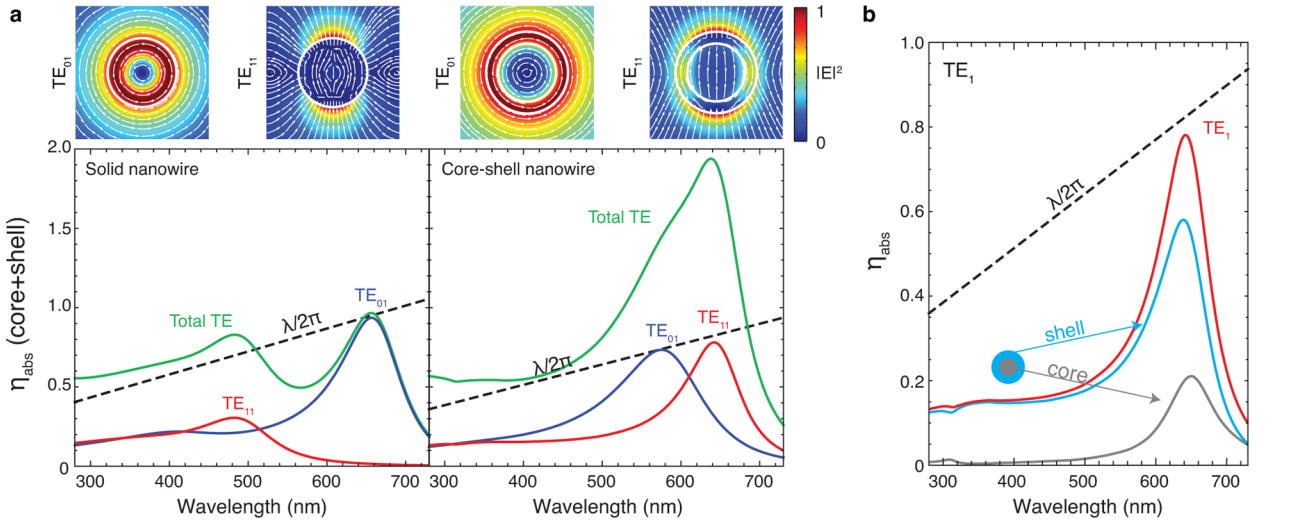

Figure 5. (a) Absorption efficiency spectra for a 110 nm diameter a-Si nanowire (left) and a 88 nm silver core with a 18 nm a-Si shell (right) in the TE polarization. Green shows the total absorption, blue and red the 0th and 1st order channel contributions. The color plots show the electric field intensity (with the stream plot indicating the direction of the field) for the TE_{01} and TE_{11} resonances for both the solid and core−shell nanowires. (b) Absorption efficiency spectrum in TE_1 (red) for the same nanowire but broken down into absorption in the shell (blue) and core (gray). In all figures the dashed line shows the fundamental limit to absorption in a single channel (resonant mode), $\lambda/2\pi$, normalized to the diameter of the nanowire.

band gap energy and lower refractive index (see Supporting Information, Figure S3). In fact, any combination of metals and semiconductors should benefit from this geometry as long as the metal loss is low, the semiconductor absorption coefficient has a rapid increase near the band gap (typically direct band gap materials), and the shell refractive index is high (most inorganic semiconductors).

We have thus far shown results for a limited number of ideal systems involving perfect Ag cylinders coated with common solar cell thin-film materials. The high symmetry of such model systems allows us to use Mie theory to break down the total absorption into the constituent channels. This provides deep insight into the underlying physics while minimizing calculation time. However, real nanowire core−shell structures will have a number of perturbations from our ideal calculations. First, the cross-sectional shape will likely not be circular; metal nanowires grown by the polyol process typically have a pentagonal cross section,[42] while semiconducting nanowires often have hexagonal or other complex cross sectional shapes.[43] We have used finite difference time domain (FDTD, Lumerical) simulations to confirm that, as with solid semiconducting nanowires,[26] the cross sectional shape only has minor effects on the resonant properties and absorption results (Supporting Information, Figure S4). We have also used FDTD to confirm that placing core−shell nanowires on low-index substrates like glass or plastic only leads to minor perturbations, primarily by increasing the radiative loss rate in the cavity and thus requiring a different shell thickness to maintain critically coupled resonances (Supporting Information, Figure S5).

In conclusion, we have shown that the key to increasing absorption in nanoscale systems is to increase the strength and number of resonances. We have demonstrated that a given resonance is strongest when the loss rates due to absorption and radiation (leakage from the cavity) are equal. This leads to the counterintuitive but fortunate conclusion that most resonances are typically strongest in spectral regions where the material absorbs the weakest. We have also demonstrated that inserting a silver core into semiconducting nanowires can lead to enhanced absorption in the shell material. This occurs because the core−shell geometry increases the number of nearly degenerate resonances by largely removing the polarization dependence of 1D nanowires. With relatively large metal cores and thin semiconductor shells, the standard Mie resonances transform into Fabry-Pérot-like resonances in both polarizations, which underlies this near-degeneracy. An added benefit of such a structure is that the metal core would provide an ideal local contact for photogenerated carrier extraction. In fact, our results suggest that it should be possible to couple the normally parasitic reflection and scattering from metal nanowire transparent electrodes into resonant modes to increase absorption in the ultrathin semiconductor shell. Therefore, hybrid core−shell nanowires provide an exciting set of building blocks for photovoltaic and solar fuel applications.

■ ASSOCIATED CONTENT

Supporting Information

Mie theory for infinite core-shell cylinders; calculation of the absorption loss rate γ_i; absorption and scattering efficiency of a plasmon resonance; peak absorption in TM; absorption with a cadmium telluride shell; comparison to a pentagonal wire and wires on a substrate. This material is available free of charge via the Internet at http://pubs.acs.org.

■ AUTHOR INFORMATION

Corresponding Author

*E-mail: garnett@amolf.nl.

Notes

The authors declare no competing financial interest.

■ ACKNOWLEDGMENTS

We are thankful to Richard R. Grote, Jorik van de Groep, Femius Koenderink, and Said Rodriguez for helpful discussions and to Henk-Jan Boluijt for creating the schematic drawing in Figure 1a. Furthermore we would like to acknowledge the Light

Management in New Photovoltaic Materials center at AMOLF. This work is part of the research program of the Foundation for Fundamental Research on Matter (FOM), which is part of The Netherlands Organization for Scientific Research (NWO).

REFERENCES

(1) European Photovoltaic Industry Association. Solar photovoltaics—competing in the energy sector. September 2011, Brussels. Available at http://www.epia.org/.
(2) Nocera, D. G.; Nash, M. P. Powering the planet: Chemical challenges in solar energy utilization. *Proc. Natl. Acad. Sci. U.S.A.* **2006**, *103*, 15729−15735.
(3) Chu, S.; Majumdar, A. Opportunities and challenges for a sustainable energy future. *Nature* **2012**, *488*, 294−303.
(4) Luque, A.; Hegedus, S. *Handbook of Photovoltaic Science and Engineering*; Wiley: New York, 2011.
(5) Cao, L.; White, J. S.; Park, J.-S.; Schuller, J. A.; Clemens, B. M.; Brongersma, M. L. Engineering light absorption in semiconductor nanowire devices. *Nat. Mater.* **2009**, *8*, 643−7.
(6) Garnett, E.; Yang, P. Light trapping in silicon nanowire solar cells. *Nano Lett.* **2010**, *10*, 1082−7.
(7) Kelzenberg, M. D.; Boettcher, S. W.; Petykiewicz, J. A.; Turner-Evans, D. B.; Putnam, M. C.; Warren, E. L.; Spurgeon, J. M.; Briggs, R. M.; Lewis, N. S.; Atwater, H. A. Enhanced absorption and carrier collection in Si wire arrays for photovoltaic applications. *Nat. Mater.* **2010**, *9*, 239−244.
(8) Zhu, J.; Yu, Z.; Burkhard, G. F.; Hsu, C.; Connor, S. T.; Xu, Y.; Wang, Q.; McGehee, M.; Fan, S.; Cui, Y. Optical Absorption Enhancement in Amorphous Silicon Nanowire and Nanocone Arrays. *Nano Lett.* **2009**, *9*, 279−282.
(9) Yao, Y.; Yao, J.; Narasimhan, V. K.; Ruan, Z.; Xie, C.; Fan, S.; Cui, Y. Broadband light management using low-Q whispering gallery modes in spherical nanoshells. *Nat. Commun.* **2012**, *3*, 664−670.
(10) Schuller, J. A.; Barnard, E. S.; Cai, W.; Jun, Y. C.; White, J. S.; Brongersma, M. L. Plasmonics for extreme light concentration and manipulation. *Nat. Mater.* **2010**, *9*, 193−204.
(11) Atwater, H. A.; Polman, A. Plasmonics for improved photovoltaic devices. *Nat. Mater.* **2010**, *9*, 205−213.
(12) Novotny, L.; Hecht, B. *Principles of Nano-Optics*, 2nd ed.; Cambridge University Press: New York, 2012.
(13) Mann, S. A.; Grote, R. R.; Osgood, R. M.; Schuller, J. A. Dielectric particle and void resonators for thin film solar cell textures. *Opt. Express* **2011**, *19*, 25729−257240.
(14) Garnett, E. C.; Brongersma, M. L.; Cui, Y.; McGehee, M. D. Nanowire Solar Cells. *Annu. Rev. Mater. Res.* **2011**, *41*, 269−295.
(15) Tang, J.; Huo, Z.; Brittman, S.; Gao, H.; Yang, P. Solution-processed core-shell nanowires for efficient photovoltaic cells. *Nat. Nanotechnol.* **2011**, *6*, 568−72.
(16) Tian, B.; Zheng, X.; Kempa, T. J.; Fang, Y.; Yu, N.; Yu, G.; Huang, J.; Lieber, C. M. Coaxial silicon nanowires as solar cells and nanoelectronic power sources. *Nature* **2007**, *449*, 885−9.
(17) Fan, Z.; Razavi, H.; Do, J.; Moriwaki, A.; Ergen, O.; Chueh, Y.-L.; Leu, P. W.; Ho, J. C.; Takahashi, T.; Reichertz, L. A.; Neale, S.; Yu, K.; Wu, M.; Ager, J. W.; Javey, A. Three-dimensional nanopillar-array photovoltaics on low-cost and flexible substrates. *Nat. Mater.* **2009**, *8*, 648−53.
(18) Wallentin, J.; Anttu, N.; Asoli, D.; Huffman, M.; Aberg, I.; Magnusson, M. H.; Siefer, G.; Fuss-Kailuweit, P.; Dimroth, F.; Witzigmann, B.; Xu, H. Q.; Samuelson, L.; Deppert, K.; Borgström, M. T. InP nanowire array solar cells achieving 13.8% efficiency by exceeding the ray optics limit. *Science* **2013**, *339*, 1057−1060.
(19) Krogstrup, P.; Jørgensen, H. I.; Heiss, M.; Demichel, O.; Holm, J. V.; Aagesen, M.; Nygard, J.; Fontcuberta i Morral, A. Single-nanowire solar cells beyond the Shockley-Queisser limit. *Nat. Photonics* **2013**, *7*, 306−310.
(20) Hecht, D. S.; Hu, L.; Irvin, G. Emerging transparent electrodes based on thin films of carbon nanotubes, graphene, and metallic nanostructures. *Adv. Mater.* **2011**, *23*, 1482−513.
(21) Lee, J.-Y.; Connor, S. T.; Cui, Y.; Peumans, P. Solution-Processed Metal Nanowire Mesh Transparent Electrodes. *Nano Lett.* **2008**, *8*, 689−692.
(22) Van de Groep, J.; Spinelli, P.; Polman, A. Transparent conducting silver nanowire networks. *Nano Lett.* **2012**, *12*, 3138−3144.
(23) Zhan, Y.; Zhao, J.; Zhou, C.; Alemayehu, M.; Li, Y.; Li, Y. Enhanced photon absorption of single nanowire α-Si solar cells modulated by silver core. *Opt. Express* **2012**, *20*, 11506−11516.
(24) Paniagua-Domínguez, R.; Abujetas, D. R.; Sánchez-Gil, J. A. Ultra low-loss, isotropic optical negative-index metamaterial based on hybrid metal-semiconductor nanowires. *Sci. Rep.* **2013**, *3*, 1507.
(25) Cao, L.; Fan, P.; Vasudev, A. P.; White, J. S.; Yu, Z.; Cai, W.; Schuller, J. A.; Fan, S.; Brongersma, M. L. Semiconductor nanowire optical antenna solar absorbers. *Nano Lett.* **2010**, *10*, 439−445.
(26) Yu, Y.; Ferry, V. E.; Alivisatos, A. P.; Cao, L. Dielectric core-shell optical antennas for strong solar absorption enhancement. *Nano Lett.* **2012**, *12*, 3674−3681.
(27) Kats, M. A.; Blanchard, R.; Genevet, P.; Capasso, F. Nanometre optical coatings based on strong interference effects in highly absorbing media. *Nat. Mater.* **2012**, *12*, 20−24.
(28) Dotan, H.; Kfir, O.; Sharlin, E.; Blank, O.; Gross, M.; Dumchin, I.; Ankonina, G.; Rothschild, A. Resonant light trapping in ultrathin films for water splitting. *Nat. Mater.* **2012**, *12*, 158−164.
(29) Bohren, C. F.; Huffman, D. R. *Absorption and Scattering of Light by Small Particles*; Wiley: New York, 1983.
(30) Grzela, G.; Paniagua-Domínguez, R.; Barten, T.; Fontana, Y.; Sánchez-Gil, J. A.; Gómez Rivas, J. Nanowire antenna emission. *Nano Lett.* **2012**, *12*, 5481−5486.
(31) Yu, Y.; Cao, L. Coupled leaky mode theory for light absorption in 2D, 1D, and 0D semiconductor nanostructures. *Opt. Express* **2012**, *20*, 13847−13856.
(32) Palik, E. D. *Handbook of Optical Constants of Solids*, Vol. *1*; Academic: New York, 1998.
(33) Haus, H. A., *Waves and Fields in Optoelectronics*; Prentice-Hall: Englewood Cliffs, NJ, 1984.
(34) Ruan, Z.; Fan, S. Superscattering of Light from Subwavelength Nanostructures. *Phys. Rev. Lett.* **2010**, *105*, 013901.
(35) Hamam, R. E.; Karalis, A.; Joannopoulos, J. D. Coupled-mode theory for general free-space resonant scattering of waves. *Phys. Rev. A* **2007**, *75*, 053801.
(36) Schuller, J. A.; Taubner, T.; Brongersma, M. L. Optical antenna thermal emitters. *Nat. Photonics* **2009**, *3*, 658−661.
(37) Yu, Z.; Raman, A.; Fan, S. Fundamental limit of nanophotonic light trapping in solar cells. *Proc. Natl. Acad. Sci. U.S.A.* **2010**, *107*, 17491−17496.
(38) ASTM G173-03, *Terrestrial reference spectra for photovoltaic performance evaluation*; American Society for Testing and Materials: West Conshohocken, PA, 2012.
(39) Schuller, J. A.; Brongersma, M. L. General properties of dielectric optical antennas. *Opt. Express* **2009**, *17*, 24084−24095.
(40) Bambino, T. M.; Breitschaft, A. M. S.; Barbosa, V. C.; Guimarães, L. G. Application of semiclassical and geometrical optics theories to resonant modes of a coated sphere. *J. Opt. Soc. Am. A* **2003**, *20*, 489−98.
(41) Catrysse, P. B.; Fan, S. Understanding the dispersion of coaxial plasmonic structures through a connection with the planar metal-insulator-metal geometry. *Appl. Phys. Lett.* **2009**, *94*, 231111.
(42) Wiley, B.; Sun, Y.; Xia, Y. Synthesis of silver nanostructures with controlled shapes and properties. *Acc. Chem. Res.* **2007**, *40*, 1067−1076.
(43) Kim, S.-K.; Day, R. W.; Cahoon, J. F.; Kempa, T. J.; Song, K.-D.; Park, H.-G.; Lieber, C. M. Tuning light absorption in core/shell silicon nanowire photovoltaic devices through morphological design. *Nano Lett.* **2012**, *12*, 4971−4976.

dx.doi.org/10.1021/nl401179h | *Nano Lett.* XXXX, XXX, XXX−XXX